Slow acceleration and deacceleration through a Hopf bifurcation: Power ramps, target nucleation, and elliptic bursting

Steven M. Baer*
Department of Mathematics and Statistics, Center of Adaptive Neural Systems, Arizona State University, Tempe, Arizona 85287, USA

Erin M. Gaekel
Harrington Department of Bioengineering, Arizona State University, Tempe, Arizona 85287, USA
(Received 5 June 2008; published 5 September 2008)

From the periodicity of regional climate change to sustained oscillations in living cells, the transition between stationary and oscillatory behavior is often through a Hopf bifurcation. When a parameter slowly passes or ramps through a Hopf bifurcation there is a delayed transition to sustained oscillations and an associated memory effect where onset is dependent on the initial state of the system. Most theoretical studies of the delay and memory effect assume constant ramp speeds, overlooking the problem of slow parameter acceleration or deacceleration through the Hopf bifurcation. Using both numerical and analytic methods, we show that slow nonlinear ramps can significantly increase or decrease the onset threshold, changing profoundly our understanding of the associated memory effect. We found that slow parameter acceleration increases the threshold, whereas slow deacceleration decreases the threshold. The theory is applied to the formation of pacemakers in the unstirred Belousov-Zhabotinsky reaction and the onset of elliptic bursting in the context of nerve membrane excitability. We show that our results generalize to all systems where slow passage through a Hopf bifurcation is the underlying mechanism for onset.

DOI: 10.1103/PhysRevE.78.036205 PACS number(s): 05.45.−a, 82.39.−k, 87.10.−e

I. INTRODUCTION

In many biological, chemical, and physical systems modeled mathematically as bifurcation problems, the bifurcation parameter may vary naturally and slowly in time or the parameter may be slowly varied by the experimenter. These are called slow passage or dynamic bifurcation problems. Of particular interest is when the dynamic parameter passes slowly through a Hopf bifurcation before transitioning to large sustained oscillations. The interesting phenomena is that this transition may not occur until the parameter is considerably beyond the value predicted from a static bifurcation analysis (delay effect), and that the delay in onset is dependent on the initial state of the system (memory effect). Numerous studies have focused on linear or constant speed ramps [1–5] and the influence of stochastic fluctuations on the onset of oscillations [3,4,6–8].

Inherent to biological, chemical, and physical systems, but often overlooked or misunderstood in the literature are nonlinear ramp problems where a parameter or variable slowly accelerates or deaccelerates through bifurcation points. An example from physics is the dynamics of laser oscillations in response to the slow nonlinear increase in small amplitude noise [9]. Nonlinear ramps involving a Hopf transition from steady to oscillatory behavior occur in fast-spiking cortical neurons [10], "spontaneous" formation of "pacemaker" centers in chemical reactions [11,12], and burst dynamics [13,14]. To date, most reported examples associated with experiment involve slowly increasing saturating exponential parameters or variables; that is, slowly increasing but deaccelerating ramps.

*baer@math.la.asu.edu

In this paper we investigate numerically and analytically the slow passage of nonlinear monotonic ramps through a Hopf bifurcation, and apply the results to accommodation in nerves, target nucleation in chemical reactions, and neuronal elliptic bursting. The plan of the paper is as follows. In Sec. II we illustrate nonlinear ramping on the well known FitzHugh-Nagumo equation and compare the dynamics to linear ramps. In Sec. III the onset integral condition for general slow monotonic ramps is studied. The integral condition is derived in the Appendix using WKB analysis. In Secs. IV and V we apply the onset condition to explain in detail onset of target nucleation in chemical reactions, and to quantify analytically silent phase duration in neuronal elliptic burst dynamics.

II. POWER RAMPS: DELAY AND MEMORY EFFECTS

Figure 1 illustrates the delay effect for the FitzHugh-Nagumo (FHN) model of nerve membrane excitability

$$\frac{dv}{dt} = -v(v-a)(v-1) - w + I(\epsilon t), \tag{1}$$

$$\frac{dw}{dt} = b(v - \gamma w). \tag{2}$$

Here, $I(\epsilon t)=I_0+(\epsilon t)^P$ $(P>0,\ \epsilon \ll 1)$, is a slowly increasing applied current. The membrane potential v is the main observable, w models a slow recovery current, a, b, γ are kinetic parameters. When I is treated as a static bifurcation parameter $(\epsilon=0)$, the bifurcation structure displayed in Figs. 1(a)–1(c) is computed numerically [15]. The static or reference Hopf bifurcation point is denoted by I_H. The current I_j denotes the jump to the oscillatory state, defined here nu-

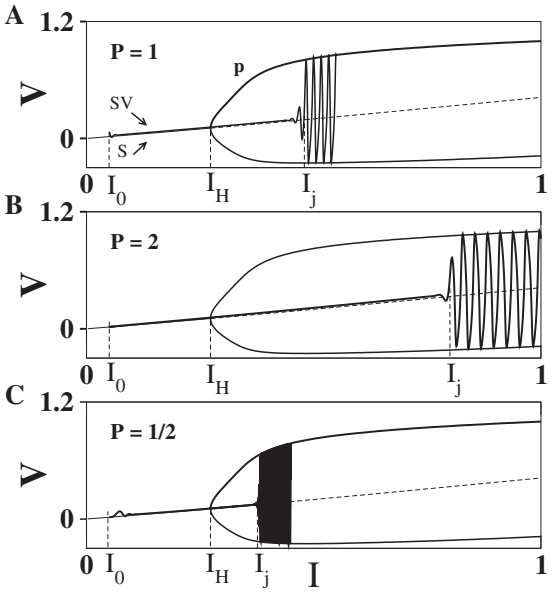

FIG. 1. Delayed onset of oscillations for linear, accelerated, and deaccelerated power ramps. The membrane potential trajectory for the FitzHugh-Nagumo model ($a=0.2$, $b=0.05$, $\gamma=0.4$) is plotted as a function of the stimulus current $I(\epsilon t)=I_0+(\epsilon t)^P$, for $P=1,2,1/2$. Superimposed for reference is the bifurcation structure for steady-state (S) and periodic (p) solutions when I is treated as a static bifurcation parameter in the governing equations. Slowly varying trajectories (SV) initiate from $I_0=0.05$ and pass through the reference Hopf point $I_H\approx 0.273$ before jumping to periodic solutions at I_j. (A) For a slow linear (constant speed) ramp ($P=1$, $\epsilon=5\times10^{-4}$) onset occurs when $I_j-I_H\approx I_H-I_0$ as found in previous studies. (B) For a slow accelerating ramp ($P=2$, $\epsilon=5\times10^{-4}$) the delay to onset is significantly increased: $I_j-I_H\approx 2(I_H-I_0)$. (C) A slow deaccelerating ramp ($P=1/2$, $\epsilon=0.5\times10^{-4}$) significantly decreases the delay to onset: $I_j-I_H\approx\frac{1}{2}(I_H-I_0)$.

merically as simply the value of current corresponding to when the potential exceeds $v=0.4$. Superimposed are the trajectories for constant speed ($P=1$), accelerating ($P=2$) and deaccelerating ($P=1/2$) ramps. In all three cases there is a delay to onset; the trajectories initiating from I_0, pass slowly through I_H and jump to the oscillatory state at I_j. Figure 1(a) illustrates the well known case of the linear ramp. The onset of oscillations occurs when I_H is approximately midway between I_0 and I_j. This is in stark contrast to the slow accelerating ramp in Fig. 1(b) where the delay to onset is doubled, or the slow deaccelerating ramp it Fig. 1(c) where the delay is halved.

The memory effect is illustrated in Fig. 2 for the FHN system. The relation I_j-I_H versus I_H-I_0 is plotted for hundreds of different initial currents I_0. Also plotted are lines $I_j-I_H=P(I_H-I_0)$, for P=$\frac{1}{2}$, 1, and 2. For $I_H-I_0>0.1$, the lines provide good approximations to the numerical solutions. In fact, a simple but remarkable application of the Wentzel-Kramers-Brillouin (WKB) approximation (see the Appendix and next section) reveals that ramps of the form $I(\epsilon t)=I_0+(\epsilon t)^P$, for any $P>0$, have the onset condition

$$I_j - I_H = P(I_H - I_0), \quad P > 0, \tag{3}$$

as $\epsilon\to 0$, if the real part of eigenvalues $\lambda(I)$, for Eqs. (1) and (2) linearized (for static I), is approximately linear over the

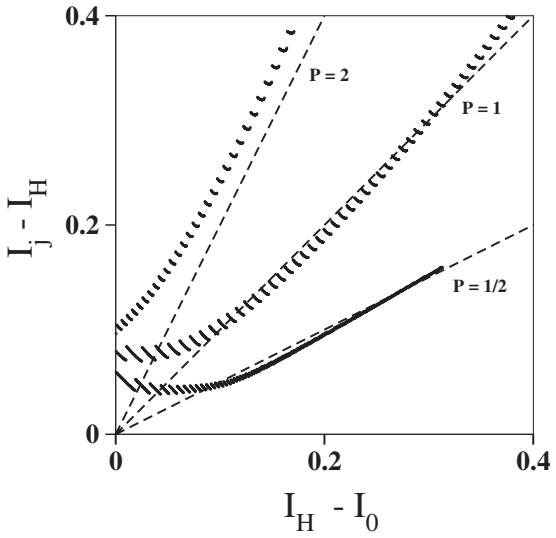

FIG. 2. The memory effect for linear ($P=1$), accelerated ($P=2$), and deaccelerated ($P=1/2$) power ramps $I(\epsilon t)=I_0+(\epsilon t)^P$. Onset I_j, computed numerically for many values of I_0, is defined as the current at time t_j when the v vs t trajectory first crosses the prescribed "threshold" $v=0.4$. Superimposed (dashed) are the predicted values of I_j using the WKB approximation $I_j-I_H=P(I_H-I_0)$. Same parameters as in Fig. 1.

range of the ramp. For $I_H-I_0<0.1$ the numerics for all three cases deviate from the WKB prediction. This is due in part to the bifurcation being supercritical when I_0 is near I_H; several small oscillations are required to bring the potential to the prescribed "threshold" [4]. Even for more precise definitions of the numerical threshold, there will always be a small saturation effect for $I_H-I_0\ll 0.1$ since the trajectory is too close to the Hopf point for it to relax to the stable steady state. Finally, it is important to point out that small amplitude noise or periodic environmental fluctuations of near resonant frequencies may decrease the delay or destroy the memory effect [4,6].

III. ONSET CONDITIONS FOR NONLINEAR MONOTONIC RAMPS

A more general class of functions can also give rise to delays and memory effects. Consider the slow ramp $I(\epsilon t)=I_0+g(\epsilon t)$, where $g(0)=0$ and $g(\epsilon t)$ is a monotonic increasing function. The onset condition (see the Appendix) for oscillations is

$$\int_{I_0}^{I_j} [g^{-1}(I-I_0)]' \{\mathrm{Re}\,\lambda(I)\}_{\max} dI = 0, \tag{4}$$

where $[g^{-1}(I-I_0)]'$ is the derivative of g inverse. The expression $\{\mathrm{Re}\,\lambda(I)\}_{\max}$ denotes the maximum real part of eigenvalue λ computed from the linearization of the differential equation system for constant I. At the Hopf point $\{\mathrm{Re}\,\lambda(I)\}_{\max}=0$, but $\mathrm{Im}[\lambda(I)]\neq 0$ and $\frac{d\{\mathrm{Re}\,\lambda(I)\}_{\max}}{dI}>0$. Destabilization of the slowly varying solution does not occur at I_H, but only after the integrated effect of $[g^{-1}(I-I_0)]'\{\mathrm{Re}\,\lambda(I)\}_{\max}>0$ overcomes the accumulated influence of

$[g^{-1}(I-I_0)]'$ $\{\mathrm{Re}\,\lambda(I)\}_{\max}<0$. Moreover, as in previous WKB analyses [4], Eq. (4) is independent of ϵ, so the delay persists no matter how slow the ramp is rising. For a linear ramp ($I=I_0+\epsilon t$), the inverse function $[g^{-1}(I-I_0)]'=1$ and condition (4) reduces to $\int_{I_0}^{I_j}\{\mathrm{Re}\,\lambda(I)\}_{\max}\,dI=0$, the condition found in previous studies including steady bifurcation problems [16,17].

It is useful to point out that for monotonic ramps, onset condition (4) reduces to

$$\int_0^{t_j}\{\mathrm{Re}\,\lambda(I(t))\}_{\max}dt=0, \tag{5}$$

which should not be confused with Eq. (3.13a) in Ref. [4]. The two integrals look the same, but in Ref. [4] the integral is in terms of the scaled variable τ, whereas Eq. (5) is in terms of physical time t. To derive Eq. (5) substitute into Eq. (4) the change of variables $I-I_0=\tau$, where $\tau=g(u)$ for $u=\epsilon t$, and use the fact that $[g^{-1}(\tau)]'=1/g'(u)$. Note that the derivation of Eq. (5) from Eq. (4) involves $g'(u)$ appearing in the denominator, which would be problematic for nonmonotonic ramps.

For many systems, $\{\mathrm{Re}\,\lambda(I)\}_{\max}\approx\bar{\lambda}'$ $(I-I_H)$, where $\bar{\lambda}'=\frac{d\{\mathrm{Re}\,\lambda(I)\}_{\max}}{dI}\big|_{I=I_H}$, over the range of the ramp. This is the case for the FHN equation and the FitzHugh-Rinzel (FHR) burster discussed later. Substituting this approximation into condition (4) and then integrating by parts, the onset condition becomes

$$(I_j-I_H)g^{-1}(I_j-I_0)=\int_{I_0}^{I_j}g^{-1}(I-I_0)dI. \tag{6}$$

The simplest application of condition (6) is for power ramps $I=I_0+(\epsilon t)^P$, $P>0$. Here $g(\epsilon t)=(\epsilon t)^p$ and therefore $g^{-1}(I-I_0)=(I-I_0)^{1/P}$. Substituting $g^{-1}(I-I_0)$ and $g^{-1}(I_j-I_0)$ into Eq. (6), integrating and simplifying leads to Eq. (3), namely, $I_j-I_H=P(I_H-I_0)$, for $P>0$. Note that relative to a linear ramp ($P=1$) an accelerating ramp ($P>1$) increases I_j threshold whereas a deaccelerating ramp ($P<1$) decreases the onset threshold.

IV. TARGET NUCLEATION

In many applications the bifurcation parameter varies naturally with time and the ramp dynamics are generated by a slow subsystem that either explicitly drives the fast subsystem or is bidirectionally coupled to the fast subsystem. One example of an explicitly driven system is the "spontaneous" formation of "pacemaker" centers in the unstirred, ferroin $[\mathrm{Fe(phen)}_3^{2+}/\mathrm{Fe(phen)}_3^{3+}]$-catalyzed Belousov-Zhabotinsky (BZ) reaction [18]. In an extension of the Oregonator model, Sobel *et al.* [11] derived a reduced model for capturing qualitative BZ kinetics in the auto-oscillatory

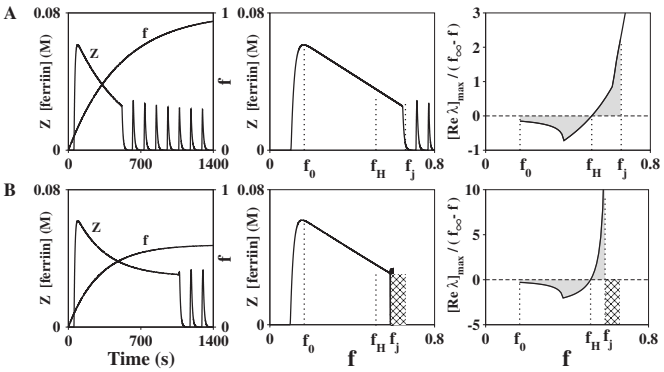

FIG. 3. The dynamical structure of the stoichiometric factor f, in the Oregonator model, determines the induction period to chemical oscillations. (A) Parameters (see below) are identical to Fig. 1 ($c=0$ case) in Ref. [11]. Left: Superimposed is the evolution of stoichiometric factor f (right axis) and ferriin (z). with no added initial conditions: $x=0$, $y=0.001$, $z=0$, and $f=0$. Center: The oxidized induction period (high ferriin) begins when $f=f_0$ (≈ 0.167). As ferriin decreases, f slowly increases through the static Hopf point f_H (≈ 0.515). At $f=f_j$ the ferriin "crashes." Right: The value $f_j\approx 0.6896$ is determined analytically from onset condition (4), as the point where the grey area above zero (dashed line) is equal to the grey area below zero. (B) The shape of f is changed while preserving the initial value f_0 of the oxidized induction period. Reducing the saturation level of f prolongs the induction period (left) but decreases f_j (center) as predicted from the onset condition (right). With no added Br^- release, the static Hopf point f_H is independent of the form of f. Parameter values: $k_c=1$, $[H^+]=0.316$ M, $[MA]_0=0.10$ M, $[BrO_3]=0.25$ M, $k_2=3\times 10^6$ M^{-2} s^{-1}, $k_3=2$ M^{-3} s^{-1}, $k_4=1500$ M^{-1} s^{-1}, and $k_5=42$ M^{-2} s^{-1}. Above in (A), $k_f=0.002$ s^{-1}, $f_\infty=1$; in (B), $k_f=0.00333$ s^{-1}, $f_\infty=0.6$.

regime. For the case of no added Br^- release, the equations are

$$\frac{dx}{dt}=k_3[BrO_3^-][H^+]^2y-k_2[H^+]xy+k_5[BrO_3^-][H^+]x-2k_4x^2, \tag{7}$$

$$\frac{dy}{dt}=-k_3[BrO_3^-][H^+]^2y-k_2[H^+]xy+(f/2)k_c[MA]_0z, \tag{8}$$

$$\frac{dz}{dt}=2k_5[BrO_3^-][H^+]x-k_c[MA]_0z, \tag{9}$$

$$\frac{df}{dt}=k_f(f_\infty-f). \tag{10}$$

Here, x,y,z denote the concentrations of $HBrO_2$, Br^-, and ferriin, respectively; and f is a slowly varying stoichiometric factor. Detailed definitions of all parameters in Eqs. (7)–(10) are given in Ref. [11]. When f is treated as a static bifurcation parameter there exists, at a critical value of f, a Hopf bifurcation from a blue oxidized steady state to an oscillatory (blue/red) state. When f is dynamic and governed by Eq. (10), the onset of oscillations is delayed, providing a demonstration of target nucleation in the supercritical regime

[11,12]. The solution to Eq. (10) is the slowly rising saturating exponential function

$$f(t) = f_\infty(1 - e^{-k_f t}), \quad t \geqslant 0. \tag{11}$$

Figure 3 (left and center) shows the dynamics of ferriin (variable z) as f increases from its initial value of $f=0$ to $f=f_\infty$ for the case of no added Br^- release ($c=0$ in [11]). In both Figs. 3(a) and 3(b) the oxidized induction period (high ferriin) initiates at $t_0 \approx 53$ s ($f_0 \approx 0.167$). The computations in Fig. 3(a) (left and center) correspond to Fig. 1 ($c=0$) in Ref. [11]. We numerically integrate Eqs. (7)–(10) using a fourth-order Runge-Kutta method ($\Delta t = 5 \times 10^{-4}$) in quadruple precision to reduce the effect of roundoff error [3,4]. This accounts for why the computed delay to onset in Fig. 3(a) (center) is longer (by about 40 s) than the delay reported in Ref. [11]. In Fig. 3(b) we further deaccelerate f while keeping f_0, the initial value of the induction period, fixed. This is accomplished by slightly increasing k_f but reducing the saturation level f_∞ by 40%. Increasing the deacceleration of the ramp decreases the onset threshold f_j [Fig. 3(b) center] by the amount shown in the crosshatched area. Note that the linearization of Eqs. (7)–(9) is independent of changes in k_f and f_∞ and therefore the value of f at the Hopf point, $f_H \approx 0.515$, remains unchanged.

The more general condition (4) is required to obtain an analytic prediction of f_j, corresponding to the onset of oscillations. To apply this condition we must first rewrite Eq. (11), so that $t=t_0$ corresponds to $f=f_0$:

$$f(t) = f_0 + (f_\infty - f_0)(1 - e^{-k_f(t-t_0)}), \quad t \geqslant t_0. \tag{12}$$

Next, we introduce the change of variables $t=s+t_0$ and $\tilde{f}(s) = f(s+t_0)$ to obtain the induction period ramp

$$\tilde{f} = f_0 + g(u), \quad u = k_f s, \tag{13}$$

where $g(u)=(f_\infty - f_0)(1-e^{-u})$. Note that $g(0)=0$, and $g(u)$ is a monotonic increasing function with inverse $g^{-1}(u) = \ln(\frac{f_\infty - f_0}{f_\infty - f_0 - u})$. Finally, we substitute the derivative of $g^{-1}(u)$, evaluated at $u=f-f_0$, into onset condition (4) to obtain

$$\int_{f_0}^{f_j} \frac{\{\mathrm{Re}\,\lambda(f)\}_{\max}}{f_\infty - f} df = 0. \tag{14}$$

Here $\{\mathrm{Re}\,\lambda(f)\}_{\max}$ is the maximum of the real part of the eigenvalues from the linearization of Eqs. (7)–(9) for static values of f.

To determine f_j, the integrand of Eq. (14) is plotted versus f in the right panels of Fig. 3. The eigenvalues $\{\mathrm{Re}\,\lambda(f)\}_{\max}$ were computed using the computer program AUTO [19]. In Fig. 3 (right) the cusps at $f \approx 0.4$, and in Fig. 3(a) the cusp at $f \approx 0.6$, are where the maximum eigenvalues switch between complex and real values. The "crash" value f_j is simply the value of f where the accumulated area in grey above zero (dashed line) is equal to the grey area below zero. Thus, condition (14) predicts $f_j \approx 0.6583$ in Fig. 3(a) (right) and $f_j \approx 0.5865$ in Fig. 3(b) (right), both within 2% relative error of the numerically computed results (center).

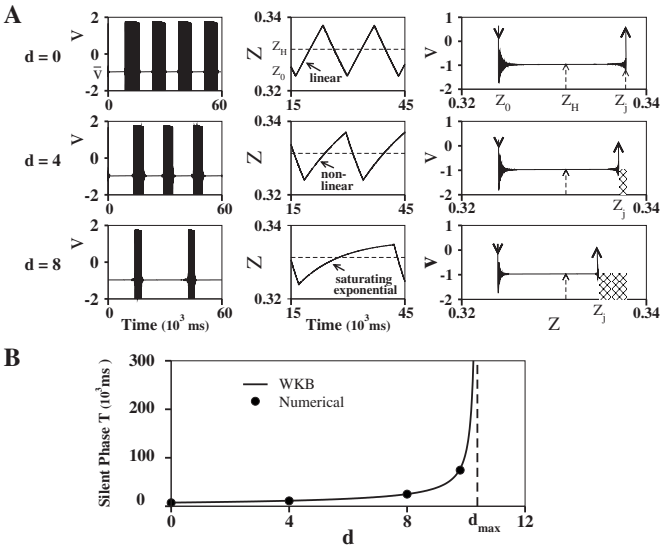

FIG. 4. Slow deaccelerating ramps influence the duration of the silent phase in deterministic elliptic bursting. (A) Left: In the FitzHugh-Rinzel model of elliptic bursting [Eqs. (15)–(17)], as parameter d increases, the duration of the silent phase increases. Center: During the silent phase Z slowly increases. The trajectory is linear for $d=0$, but nonlinear (slowly deaccelerating) for $d=4$ and $d=8$. In all three cases the trajectory ramps above the reference Hopf point Z_H (dashed line). Right: As d increases, the value Z_j marking the end of the silent phase decreases by the amount indicated by the crosshatched region. Parameter values for the FHR system are $c=-0.775$, $I=0.3125$, $\phi=0.08$, $a=0.7$, $b=0.8$, $\epsilon = 0.1 \times 10^{-4}$, and the reference Hopf value is $Z_H \approx 0.33128$. During the silent phase the approximate membrane potential is $\bar{v}=-0.97$ and initially $Z_0 \approx 0.3239$. (B) Analytic versus numerical estimates of silent phase duration. Silent phase durations T, for $d=0,4,8,9.8$, are computed numerically from the FitzHugh-Rinzel equations (black dots). Superimposed (solid curve) is the WKB approximation of T versus d. The silent phase grows without bound as d approaches $d_{\max} \approx 10.3828$.

Comparisons of Figs. 3(a) and 3(b) illustrate that slowing down the ramp, by increased deacceleration, postpones the onset of oscillations from $t_j \approx 515$ s [Fig. 3(a), left] to $t_j \approx 1074$ seconds [Fig. 3(b), left]. However, the onset value f_j decreases by the amount indicated by the crosshatched region in Fig. 3(b) (center and right). Hence, increased deacceleration reduces the threshold for onset, which is consistent with the results found for deaccelerating ($P<1$) power ramps. Hence, the dynamic structure of the ramp strongly influences the onset of oscillations.

V. ELLIPTIC BURSTING

An example where the slow system is bi-directionally coupled to the fast subsystem is elliptic bursting [20]. Figure 4(a) shows that the underlying dynamics of elliptic bursting is the slow passage of a variable through a Hopf bifurcation. Overlooked in the literature is that the dynamics of the slow variable (here a saturating exponential) contributes to the duration of the burst's silent phase. To illustrate this, consider the FitzHugh-Rinzel (FHR) model for elliptic bursting, with Z substituted for $y+I$ in Rinzel [13]:

$$\frac{dv}{dt} = v - \frac{v^3}{3} - w + Z, \tag{15}$$

$$\frac{dw}{dt} = \phi(v + a - bw), \tag{16}$$

$$\frac{dZ}{dt} = \epsilon(-v + c + Id - dZ). \tag{17}$$

Here, the fast subsystem is composed of Eqs. (15) and (16) and the slow subsystem is simply Eq. (17) for Z. The slow equation is driven by the membrane potential v and the recovery variable w while the slow variable Z drives the fast subsystem through Eq. (15). Figure 4(a) (left) shows burst trajectories for three different values of parameter d. The burst consists of two phases, an active phase characterized by large amplitude spiking and a silent phase characterized by a slowly varying steady state. After exiting the active phase, the trajectory moves slowly to the right as it spirals into the stable steady state. After passing through the static Hopf point the trajectory begins to slowly unwind about the unstable steady state until it destabilizes into large amplitude spikes. The slow ramp of Z is shown in the center panels. During the silent phase Z is monotonically increasing; linear for $d=0$, but a saturating exponential for $d=4$ and 8. As d increases, the onset of a new active phase, denoted by Z_j, decreases by the amounts shown in the crosshatched areas of Fig. 4(a) (right). As in the case of target nucleation, the reduction in threshold is due to the deaccelerating dynamics of the ramp (compare, for example, Fig. 3).

To predict analytically the duration T of the burst's silent phase as a function of d, we make the following observations. First, the real part of the eigenvalues for the fast subsystem (15) and (16) are approximately linear over the range of the silent phase, and therefore the Re λ may be approximated by Re $\lambda \approx \bar{\lambda}'(Z-Z_H)$, where $\bar{\lambda}'$ is the slope of the Re λ, and Z_H is the Hopf bifurcation point computed from the fast subsystem for Z static. Second, during the silent phase, the potential is approximately constant [see Fig. 4(a) left] and its value $\bar{v}$ is independent of d. Third, each silent phase begins at approximately the same value of Z [see Fig. 4(a) center] and this value is also independent of d. Thus, if we denote $t=0$ as the beginning of a silent phase, then the slow equation (17) reduces to the following initial value problem:

$$\frac{dZ}{dt} = \epsilon(-\bar{v} + c + Id - dZ), \quad Z(0) = Z_0. \tag{18}$$

The solution to Eq. (18) is

$$Z = Z_0 + (Z_\infty - Z_0)(1 - e^{-(\epsilon d)t}), \tag{19}$$

where

$$Z_\infty = I + \frac{c - \bar{v}}{d} \tag{20}$$

is the steady-state value of Z. Increasing d decreases Z_∞, which has the effect of further deaccelerating Z. As Z_∞ approaches Z_H, the duration of the silent phase becomes infinite. Substituting Z_H for Z_∞ in Eq. (20) and solving for d provides an estimate of $d_{\max}$; that is, $d_{\max} = (c-\bar{v})/(Z_H - I)$ is the critical value for which the duration of the silent phase becomes infinite. At $d=0$, the slow equation (17) is $dZ/dt = \epsilon(-\bar{v}+c)$ and the ramp is linear as displayed in Fig. 4(a) center (for $d=0$). For $0 < d < d_{\max}$, the silent phase ramp is a saturating exponential of the form

$$Z = Z_0 + g(u), \quad u = (\epsilon d)t, \tag{21}$$

where now $g(u) = (Z_\infty - Z_0)(1 - e^{-u})$. Again, g is monotonic with $g(0)=0$. The inverse of g evaluated at $Z - Z_0$ is

$$g^{-1}(Z - Z_0) = \ln\left(\frac{Z_\infty - Z_0}{Z_\infty - Z}\right). \tag{22}$$

To compute the duration of the silent phase, first substitute Eq. (22) into Eq. (6) and replace I_0, I_j, and I_H by Z_0, Z_j, and Z_H. The onset condition reduces, after some algebra, to the equation

$$Z_j - Z_H = (Z_\infty - Z_H) - (Z_\infty - Z_0)e^{-[(Z_j - Z_0)/(Z_\infty - Z_H)]}. \tag{23}$$

Next, we solve Eq. (23) numerically for Z_j and the duration of the silent phase is calculated by substituting Z_j into the expression

$$T = \frac{1}{\epsilon d} \ln\left(\frac{Z_\infty - Z_0}{Z_\infty - Z_j}\right), \tag{24}$$

found by backsolving explicitly for t in Eq. (19). Figure 4(b) (solid curve) plots the duration of the silent phase T versus d over $0 < d < d_{\max}$ for the parameter values given in Fig. 4. The superimposed (black dots) are the duration times obtained by numerically solving Eqs. (15)–(17), for $d=0$, 4, and 8. Both analytic and numerical estimates of the silent phase duration are in excellent agreement.

VI. CONCLUSIONS

We have shown that dynamic Hopf bifurcations are strongly influenced by the dynamic structure of slow nonlinear ramps. We have quantified how the eigenvalue structure of the associated static problem and the dynamics of the ramp jointly determine the onset of instability. We illustrated and analyzed the importance of the dynamical structure of the ramp by considering two well known examples, target nucleation in chemical reactions and neuronal elliptic bursting.

Generalizing the slow passage problem to include slow nonlinear ramps opens up the possibility for a myriad of new and potentially important research directions. One avenue is to extend the analysis and methodology to other kinds of slow passage problems, such as stochastic investigations [6–8], steady bifurcation problems [9,16,17], and dynamic Hopf problems where the ramp is from oscillatory to constant steady states [21]. Another direction for future research is the effect of more complex ramping functions, such as nonmonotonic ramps. We expect that this can be addressed by extending the methods in this report to piecewise monotonic ramps.

This study embraces and quantifies a very important concept: that a dynamical system forced by an extremely slow

process will undergo sudden destabilization as a result of slow accumulated change due jointly to the dynamic morphology of the forcing and the natural response of the system to perturbations quantified by the eigenvalues of the linearized system.

ACKNOWLEDGMENTS

We thank V.B. Pizziconi and R. Jung for helpful discussions.

APPENDIX: DERIVATION OF ONSET CONDITION (4)

Here we derive onset condition (4) for a general nth order nonlinear system of differential equations

$$\frac{d\mathbf{x}}{dt} = \mathbf{f}[\mathbf{x}, I(\epsilon t)], \tag{A1}$$

where vector $\mathbf{x}(t)$ represents n dependent variables and the vector $\mathbf{f}$ denotes the n functions for the system. The variable I is the control or bifurcation parameter, which is slowly varying in time, and of the form $I(\epsilon t)=I_0+g(\epsilon t)$ for small quantity ϵ. Additionally, we assume $g(0)=0$ and that g is a monotonic function.

For the static (constant I) case, when $\epsilon=0$, we assume that Eq. (A1) admits a basic steady-state solution $\mathbf{x}_s$ given by

$$\mathbf{f}(\mathbf{x}_s, I) = \mathbf{0}. \tag{A2}$$

The static Hopf bifurcation point is found by linearizing Eq. (A1) about the steady-state $\mathbf{x}_s$ solution, yielding

$$\frac{d\mathbf{X}}{dt} = \mathbf{J}\mathbf{X}, \tag{A3}$$

where $\mathbf{J}$ is the $n\times n$ Jacobian matrix

$$\mathbf{J} = \begin{pmatrix} \partial f_1/\partial x_1 & \partial f_1/\partial x_2 & \cdots & \partial f_1/\partial x_n \\ \partial f_2/\partial x_1 & \partial f_2/\partial x_2 & \cdots & \partial f_2/\partial x_n \\ \vdots & \vdots & \cdots & \vdots \\ \partial f_n/\partial x_1 & \partial f_n/\partial x_2 & \cdots & \partial f_n/\partial x_n \end{pmatrix} \tag{A4}$$

evaluated at $\mathbf{x}=\mathbf{x}_s$. The linearized problem has solution form $\mathbf{X}=\mathbf{Z}e^{\lambda t}$, where $\mathbf{Z}$ is a constant vector. Inserting $\mathbf{X}$ into Eq. (A3) yields the eigenvalue equation

$$\det(\mathbf{J} - \lambda\mathbf{I}) = 0, \tag{A5}$$

where $\mathbf{I}$ is the identity matrix, and exponent λ corresponds to the eigenvalues of matrix $\mathbf{J}$ evaluated at $\mathbf{x}=\mathbf{x}_s$. We assume that a single pair of eigenvalues cross the imaginary axis to change the stability of the steady state, and that at criticality these eigenvalues satisfy Im $\lambda\neq 0$ and the transversality condition $\frac{d\mathrm{Re}\,\lambda}{dI}\neq 0$ when Re $\lambda=0$. This assumption guarantees that the value $I=I_H$, for which this crossing occurs, corresponds to a Hopf bifurcation to periodic solutions. Moreover, we assume (as is the case in all our numerical simulations) that Im $\lambda(I)$ is not equal to 0 over the entire steady I of interest. The latter condition implies that we don't need to worry about turning point effects in the WKB analysis.

In applications of interest, when I is dynamic and slowly changing, the solution to Eq. (A1) often follows a trajectory that closely tracks the static steady-state solution. This slowly varying "steady-state" solution (for the nonsingular cases) can be constructed using a regular perturbation expansion of the form

$$\mathbf{x}_{sv}(\tau) \sim \mathbf{x}_0(\tau) + \epsilon\mathbf{x}_1(\tau) + \cdots \text{ as } \epsilon\to 0, \tag{A6}$$

where $\tau=g(u)$, for $u=\epsilon t$. Substituting Eq. (A6) into (A1), to leading order $\mathbf{x}_0(\tau)=\mathbf{x}_s[I(\tau)]$, and therefore $\mathbf{x}_{sv}(\tau)=\mathbf{x}_s[I(\tau)]+O(\epsilon)$. To determine when the slowly varying solution becomes unstable, we linearize Eq. (A1) about $\mathbf{x}_{sv}$, which results in a linearized system of the same form as Eq. (A3). The Jacobian matrix is identical and evaluated at $\mathbf{x}_s$, however, $\mathbf{x}_s=\mathbf{x}_s[I(\tau)]$ is now slowly varying. We substitute the Wentzel-Kramers-Brillouin (WKB) expansion

$$\mathbf{X}(t;\epsilon) \sim e^{\sigma(\tau)/\epsilon}[\mathbf{X}_0(\tau) + \epsilon\mathbf{X}_1(\tau) + \cdots] \text{ as } \epsilon\to 0 \tag{A7}$$

into the slowly varying linear system and obtain, to leading order, the algebraic problem

$$[\mathbf{J} - \sigma'(\tau)g'(u)\mathbf{I}]\mathbf{X}_0 = \mathbf{0}, \quad \mathbf{X}_0 \neq \mathbf{0}, \tag{A8}$$

where $\mathbf{J}$ is evaluated at $\mathbf{x}=\mathbf{x}_s[I(\tau)]$. System (A8) has nontrivial solutions if

$$\det[\mathbf{J} - \sigma'(\tau)g'(u)\mathbf{I}] = 0. \tag{A9}$$

Since the eigenvalue equation (A5) is identical in form to Eq. (A9),

$$\lambda = \sigma'(\tau)g'(u) \tag{A10}$$

$$= \frac{\sigma'(\tau)}{[g^{-1}(\tau)]'}, \tag{A11}$$

where $g^{-1}(\tau)$ is defined as g inverse $[u=g^{-1}(\tau)]$.

To estimate I_j, we seek the time τ_j when Re $\sigma=0$ in the WKB expansion (A7). Solving for Re σ in Eq. (A11) gives the onset condition

$$\int_0^{\tau_j} [g^{-1}(\tau)]'\{\mathrm{Re}\,\lambda(I(\tau))\}_{\max} d\tau = 0, \tag{A12}$$

where $\{\mathrm{Re}\,\lambda(I)\}_{\max}$ denotes the maximum real part of all eigenvalues λ. With the simple change of variables $I=I_0+\tau$ in Eq. (A12), we arrive at onset condition (4), namely

$$\int_{I_0}^{I_j} [g^{-1}(I-I_0)]'\{\mathrm{Re}\,\lambda(I)\}_{\max} dI = 0,$$

where $I_j=I(\tau_j)$ corresponds to the onset of large sustained oscillations.

[1] E. Jakobsson and R. Guttman, in *The Biophysical Approach to Excitable Systems*, edited by W. J. Adelman and D. E. Goldman (Plenum Press, New York, 1981), pp. 197–211.
[2] A. I. Neishtadt, Diff. Eq. **23**, 1385 (1987).
[3] J. Rinzel and S. M. Baer, Biophys. J. **54**, 551 (1987).
[4] S. M. Baer, T. Erneux and J. Rinzel, SIAM J. Appl. Math. **49**, 55 (1989).
[5] J. Z. Su, J. Differ. Equations **105**, 180 (1993).
[6] R. Kuske, J. Stat. Phys. **96**, 797 (1999).
[7] R. Kuske and S. M. Baer, Bull. Math. Biol. **64**, 447 (2002).
[8] J. Z. Su, J. Rubin, and D. Terman, Nonlinearity **17**, 133 (2004).
[9] M. Georgiou and T. Erneux, Phys. Rev. A **45**, 6636 (1992).
[10] D. Golomb, K. Donner, L. Shacham, D. Shlosberg, Y. Amitai, and D. Hansel, PLOS Comput. Biol. **3**, 1498 (2007).
[11] S. G. Sobel, H. M. Hastings, and R. J. Field, J. Phys. Chem. A **110**, 5 (2006).
[12] H. M. Hastings, R. J. Field, and S. G. Sobel, J. Chem. Phys. **119**, 3291 (2003).
[13] J. Rinzel, in *Mathematical Topics in Population Biology, Morphogenesis, and Neurosciences*, edited by E. Teramoto and M. Yamaguti (Springer, Berlin 1987), pp. 267–281.
[14] J. Best, C. Park, D. Terman, and C. Wilson, J. Comput. Neurosci. **23**, 217 (2007).
[15] B. Ermentrout, *Simulating, Analyzing, and Animating Dynamical Systems: A Guide to XPPAUT for Researchers and Students* (SIAM, Philadelphia, PA, 2002).
[16] P. Mandel and T. Erneux, Phys. Rev. Lett. **53**, 1818 (1984).
[17] R. Haberman, SIAM J. Appl. Math. **37**, 69 (1979).
[18] A. N. Zaikin and A. M. Zhabotinsky, Nature (London) **225**, 535 (1970).
[19] E. Doedel, Congr. Numer. **30**, 265 (1981).
[20] X-J Wang and J. Rinzel, in *The Handbook of Brain Theory and Neural Networks*, edited by M. Arbib (MIT Press, Cambridge, MA, 1995).
[21] L. Holden and T. Erneux, SIAM J. Appl. Math. **53**, 1045 (1993).